Biomaterials 31 (2010) 8341–8349

Contents lists available at ScienceDirect

Biomaterials

journal homepage: www.elsevier.com/locate/biomaterials

Mechanism of cell repellence on quasi-aligned nanowire arrays on Ti alloy

Lingzhou Zhao [a,c], Liangsheng Hu [b], Kaifu Huo [b,c,**], Yumei Zhang [a], Zhifen Wu [a], Paul K. Chu [c,*]

[a] School of Stomatology, The Fourth Military Medical University, No. 145 West Changle Road, Xi'an 710032, China
[b] School of Materials and Metallurgy, Wuhan University of Science and Technology, Wuhan 430081, China
[c] Department of Physics and Materials Science, City University of Hong Kong, Tat Chee Avenue, Kowloon, Hong Kong, China

ARTICLE INFO

Article history:
Received 17 May 2010
Accepted 6 July 2010
Available online 25 July 2010

Keywords:
Nanowire arrays
Wettability
Surface chemistry
Cell adhesion
Apoptosis

ABSTRACT

Cell-repelling structures are often required in biosensors, bioelectronics, and drug delivery systems, but the search for satisfactory cell-repelling structures with good biocompatibility and long-term stability is challenging. In this work, two types of quasi-aligned nanowire arrays (QANWA) with different surface chemistry but similar surface topography, namely titanium carbide–carbon core–shell (TiC/C) and titania (TiO_2), are fabricated on Ti6Al4V. Both QANWAs inhibit cell adhesion consequently leading to cell apoptosis possibly due to disruption in the adhesion assembly. Other cell functions such as proliferation and differentiation as monitored by extracellular matrix secretion and mineralization are also substantially depressed. The cell-repelling property is related to the nanostructure but independent of the surface chemistry and surface wettability. It is also not related to protein adsorption which is in fact slightly enhanced on the nanowire arrays. The QANWAs can be modified to have a larger loading capacity thereby enhancing the controlled release kinetics in drug delivery applications and to resist protein adsorption resulting in better biosensor performance. This concept which can be readily extended to other types of QANWAs and biomaterials has broad clinical potential.

1. Introduction

Better understanding of the various interactions between cells and biomaterials can expedite biomedical applications [1,2]. In particular, adhesion and subsequent functions of cells are closely related to the surface topography of biomaterials and so the proper micro- and nanotopography can modulate cells/biomaterials interactions [2]. Most of the studies have heretofore focused on factors that enhance cells/biomaterials integration to for example, improve osseo-integration between titanium implants and bones [2–5] and develop polymer scaffolds in tissue engineering applications [6,7]. In spite of recent progress, mechanisms dictating the various interactions between cells and nanostructures are still not fully understood. Better understanding of the mechanisms, particular those pertaining to negative effects such as cell repellence and apoptosis, can lead to better surface nanotopography and biomedical devices.

Surface structures that repel mammalian cell adhesion and survival have attracted increasing interest [8–12] because cell-repelling surfaces are required by many biomedical devices such as those in drug delivery and blood contacting applications as well as biosensors and bioelectronics. Besides cell repellence, high drug loading capacity and controlled release are desirable for good drug delivery, and protein resistance is required in order to keep the surface of a biosensor clean. Lee and coworkers have reported that zinc oxide (ZnO) nanorods with different surface chemistry (with or without silicon dioxide coating) effectively reduce cell adhesion and subsequent survival [8,9]. Brammer et al. have observed strikingly suppressed cell and protein adhesion on silicon nanowire arrays, suggesting that they can serve as good drug delivery carriers due to the reduced probability of biofouling and drug release impediments [10]. However, ZnO nanorods and silicon nanowires are unstable and degrade gradually in a physiological environment [13–15]. These drawbacks may stifle long-term *in vivo* and clinical uses. Hence, fabrication of a better cell-repelling surface with good biocompatibility and stability is important.

We have fabricated quasi-aligned nanowire arrays (QANWA) composed of the titanium carbide–carbon core–shell (TiC/C) structure or titania (TiO_2) on Ti6Al4V. The TiC/C and TiO_2 nanowires which have good biosensing properties have large potential in drug carrier and delivery systems because of the potentially high loading volume [10]. In order to achieve the normal functions of drug delivery systems and biosensors in a physiological environment,

* Corresponding author. Tel.: +86 852 34427724; fax: +86 852 34420542/34420538.
** Corresponding author at: School of Materials and Metallurgy, Wuhan University of Science and Technology, Wuhan 430081, China.
E-mail addresses: kfhuo@wust.edu.cn, kaifuhuo@cityu.edu.hk (K. Huo), paul.chu@cityu.edu.hk (P.K. Chu).

0142-9612/$ – see front matter © 2010 Elsevier Ltd. All rights reserved.
doi:10.1016/j.biomaterials.2010.07.036

these structures must repel cell adhesion and have an anti-biofouling surface. In this study, we report the cell-repelling property of QANWAs on Ti6Al4V. The influence of the QANWAs of TiC/C and TiO_2 on protein adsorption and cell adhesion is investigated by observing the response of osteoblasts which constitute a representative anchorage-dependent cell type to elucidate the mechanism of cell repellence.

2. Materials and methods

2.1. Fabrication of the TiC/C and TiO_2 QANWAs

Core–shell titanium carbide/carbon (TiC/C) QANWAs were fabricated by a thermochemical process as described previously (submitted for publication). In brief, Ti6Al4V foils ($10 \times 10 \times 1$ mm^3, Goodfellow) were degreased ultrasonically in acetone and ethanol sequentially, followed by polishing in a solution containing H_2O, HF, and HNO_3 with a volume ratio of 5:1:4 for 5 min to remove the surface native oxide. After rinsing with distilled water and drying under flowing nitrogen, the Ti6Al4V foil was put on a ceramic substrate placed at the center of an alumina tube in a horizontal tube furnace. The reactor was purged with argon several times to remove residual oxygen and/or moisture before being heated to 800 °C under argon. Acetone was subsequently introduced into the chamber together with argon at a flow rate of 150 sccm. The thermochemical reaction was conducted for 90 min at 800 °C and afterwards, the furnace was gradually cooled to room temperature under argon to produce the TiC/C QANWAs. The as-synthesized TiC/C QANWAs could be further transformed into TiO_2 QANWAs by annealing in air at 650 °C for 60 min. The carbon shell was removed [16] and the TiC core was converted to single-crystalline TiO_2 [17].

2.2. Surface characterization

Field-emission scanning electron microscopy (FE-SEM, FEI Nova 400 Nano) and transmission electron microscopy (TEM, JEOL JEM-2100) were used to observe the surface morphology of the specimens and structure of the nanowires, respectively. X-ray diffraction (XRD, Philips X′ Pert Pro) was employed to show the crystallization of samples. Micro Raman spectroscopy (Renishaw 2000) was conducted to determine the structure and water contact angle measurements were carried out by the sessile-drop method (EasyDrop Standard, KRUSS) at room temperature.

2.3. Protein adsorption assay

A 1 ml droplet of Dulbecco's minimum essential medium (DMEM, Gibco) containing 10% bovine calf serum (BCS, Gibco) was pipetted onto each specimen placed in 24-well plate. After incubation at 37 °C for 4 h, these disks were transferred into new 24-well plates and washed with 1000 μl PBS thrice. Afterwards, 500 μl of 1% sodium dodecyl sulfate (SDS) solution was added to these wells and shaken for 1 h to detach proteins from the disk surface. The protein concentrations in the collected SDS solutions were determined using a MicroBCA protein assay kit (Pierce).

2.4. Cell culture

Primary rat calvarial osteoblasts were obtained by digestion of calvarial bone of neonatal Sprague–Dawley rats. The cells were cultured in DMEM supplemented with 10% BCS and 1% penicillin/streptomycin and incubated in a humidified atmosphere of 5% CO_2 at 37 °C. Passages 2–5 were used in the experiments.

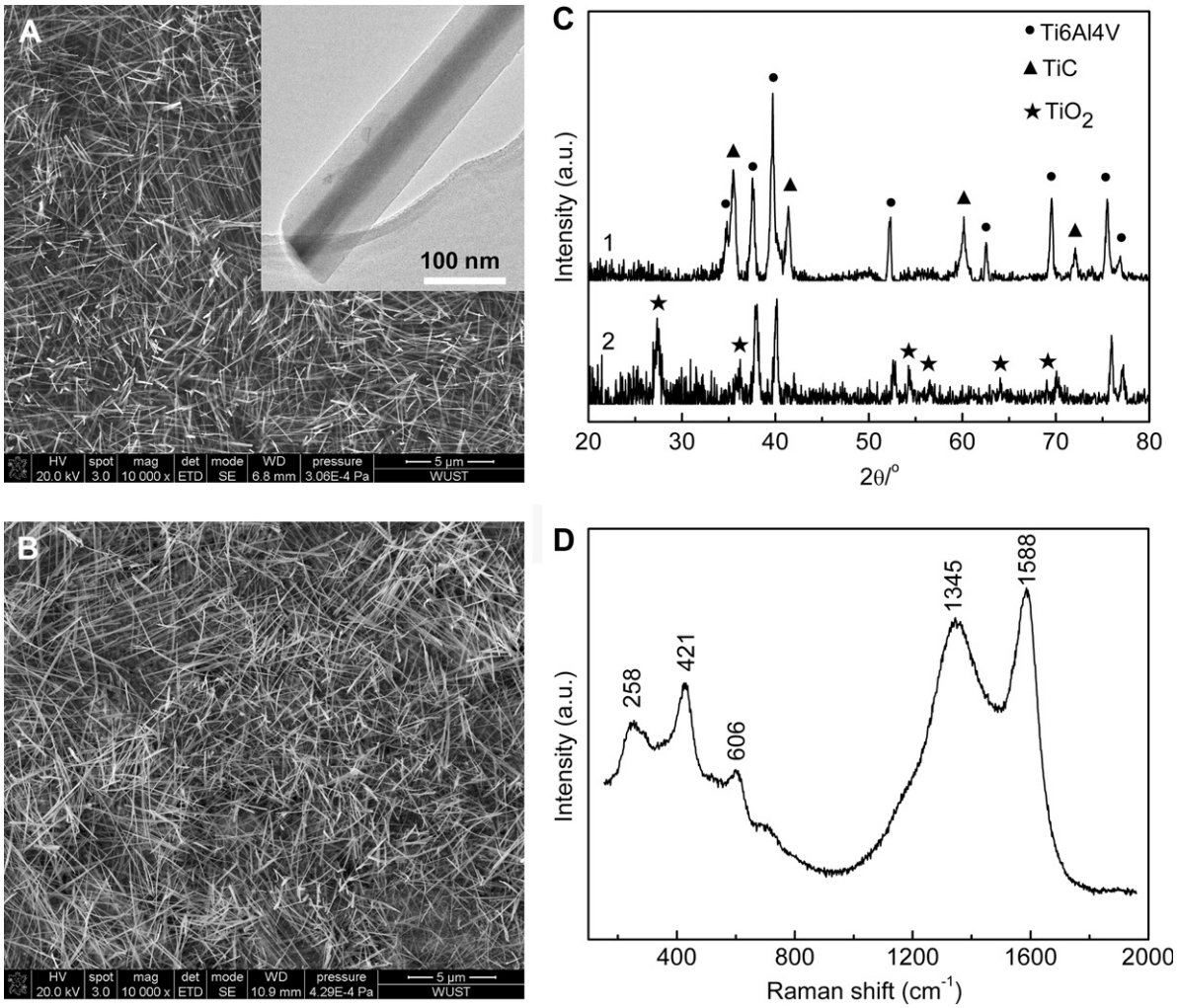

Fig. 1. SEM images of the (A) TiC/C QANWAs and (B) TiO_2 QANWAs formed by annealing TiC/C QANWAs in air at 650 °C for 60 min. The inset in (A) is the TEM picture of the TiC/C nanowire. (C) XRD patterns acquired from the TiC/C QANWAs (curve 1) and TiO_2 QANWAs (curve 2) and (D) Raman spectrum of the TiC/C QANWAs.

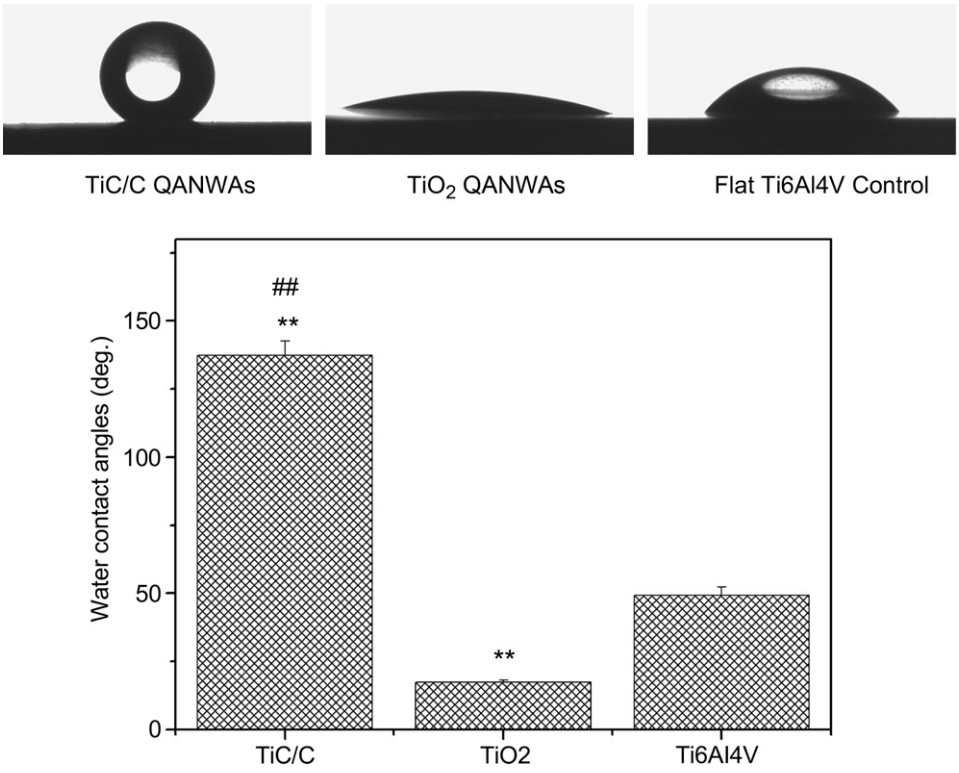

Fig. 2. Water contact angles on samples. $^{**}p < 0.01$ compared to the flat Ti6Al4V control and $^{\#\#}p < 0.01$ compared to the TiO_2 QANWAs. The top panel shows the optical pictures.

2.5. Cytotoxicity assay

The lactate dehydrogenase (LDH) activity in the culture media was used as an index of cytotoxicity. After 24 h of culturing, the culture media was collected and centrifuged, and the supernatant was used for the LDH activity assay. The LDH activity was determined spectrophotometrically according to the manufacturer's instructions.

2.6. Cell morphology

After 3 days of culturing, the samples with attached cells were gently washed with PBS and distilled water, fixed, and sputter coated with gold. The cell morphology was observed by FE-SEM (JSM-6700F).

2.7. Cell proliferation

A 1 ml droplet of cell suspension was seeded onto each specimen with a density of 2×10^4 cells/ml and then cultured in DMEM containing 10% BCS. After 1, 4, and 7 days, cell proliferation was assessed using the MTT assay. At the prescribed time points, the specimens were rinsed three times with PBS gently and transferred to a new 24-well plate. The MTT solution was added and the specimens were incubated at 37 °C to allow the formation of formazen which was then dissolved using dimethyl sulfoxide (DMSO). The optical density (OD) was measured at 490 nm using a spectrophotometer (Bio-tek).

2.8. Intracellular total protein synthesis and alkaline phosphatase activity

The cells were seeded on samples placed in 24-well culture plate with a density of 2×10^4 cells/well. After 7 days of incubation, the cells were washed with PBS thrice and lysed in 0.1% Triton X-100 through four freeze–thaw cycles. The alkaline phosphatase (ALP) activities of the samples were determined using a colorimetric assay with an ALP reagent containing p-nitrophenyl phosphate (p-NPP) as the substrate. The absorbance of p-nitrophenol was measured at 405 nm and intracellular total protein content was determined using the MicroBCA protein assay kit. The ALP activity was normalized to the protein concentration.

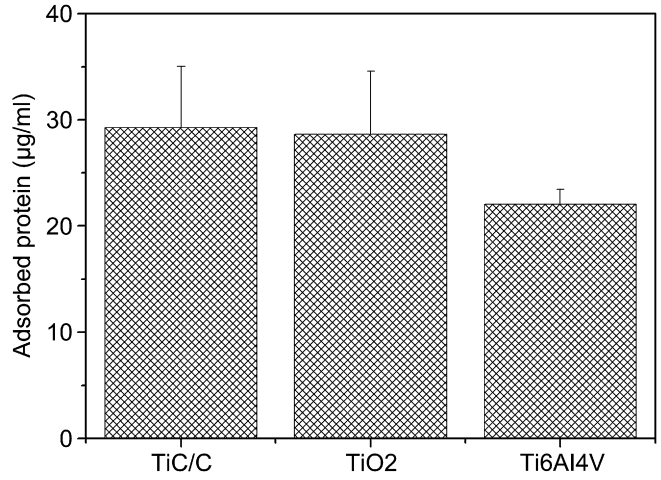

Fig. 3. Protein adsorption onto specimens after 4 h of incubation in DMEM containing 10% bovine calf serum.

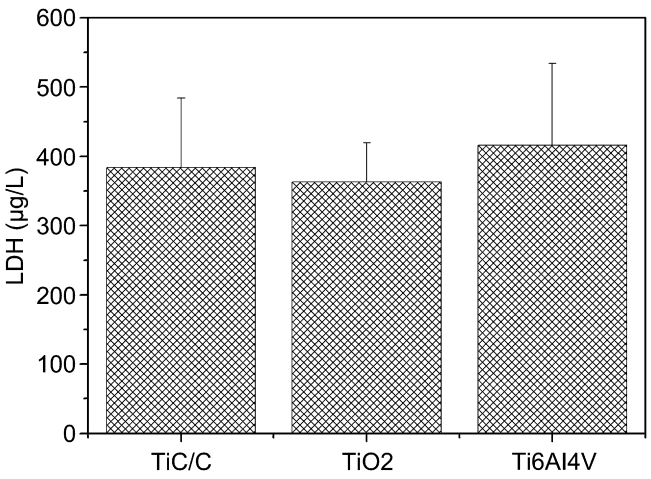

Fig. 4. Cytotoxicity assay by evaluating LDH activity in the culture media after 24 h culture of osteoblasts on the specimens.

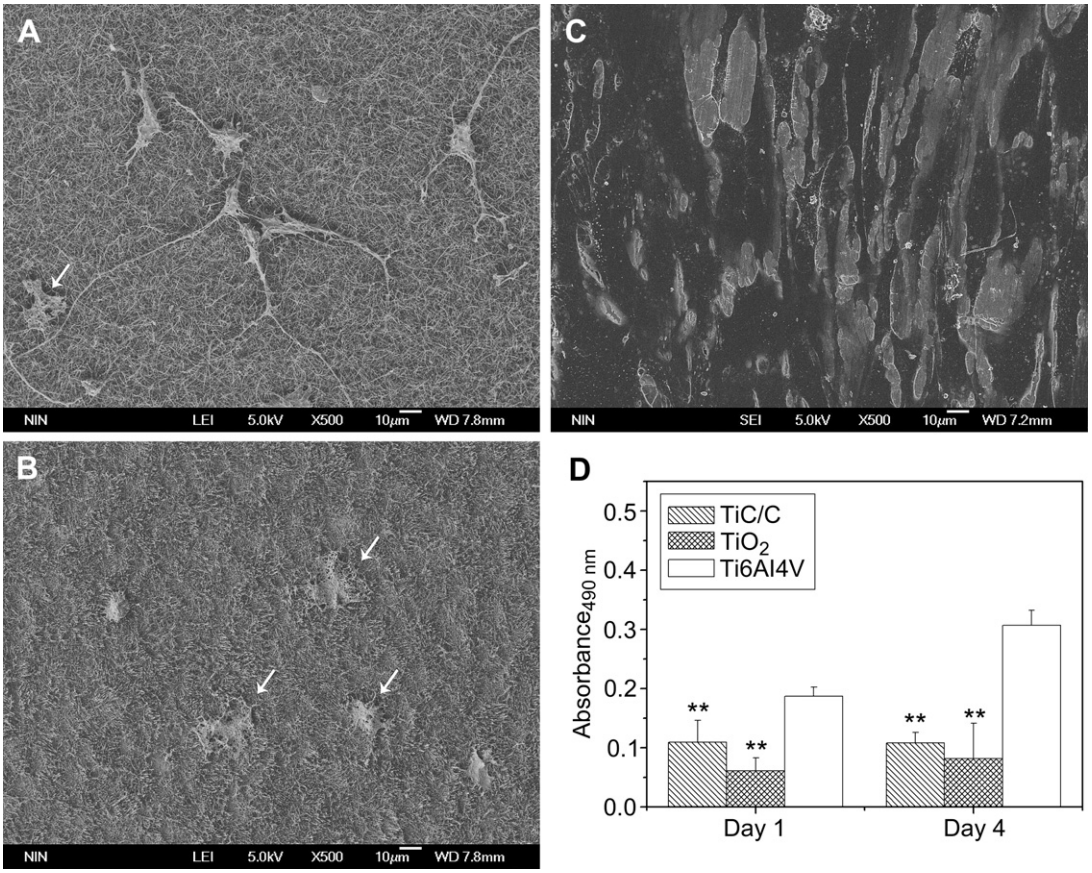

Fig. 5. SEM pictures display cell number and morphology on the specimen surfaces after an incubation period of 3 days: (A) TiC/C QANWAs; (B) TiO_2 QANWAs; (C) flat Ti6Al4V. The white arrows indicate the cells which appear to undergo apoptosis. (D) Cell proliferation after 1 and 4 days of incubation measured by the colorimetric MTT assay. $^{**}p < 0.01$ compared to the flat Ti6Al4V control.

2.9. Collagen secretion assay

Collagen secretion on the specimens was quantified using a method based on Sirius Red staining as previously described [4]. Cells with a density of 2×10^4/well were grown for 7 days, washed three times in PBS, and fixed in 4% paraformaldehyde. After three washes with PBS, the constructs were stained with a 0.1% solution of Sirius Red (Sigma) in saturated picric acid for 18 h. After washing with 0.1 M acetic acid until no more red color eluted, images were taken. For the quantitative analysis, the stain on the specimens was mixed with 500 ml of destain solution (0.2 M NaOH/methanol 1:1). The optical density at 540 nm was then measured on a spectrophotometer.

2.10. Extracellular matrix mineralization

The extracellular matrix mineralization by cells on the specimens was evaluated by Alizarin Red staining [4]. After incubation for 7 days, the cells were washed thrice with PBS and fixed with 75% ethanol for 1 h. The cell cultures were stained with 40 mM alizarin red in distilled water (pH 4.2) for 10 min at room temperature. Afterwards, the cells were washed with distilled water until they were no longer red and then images were acquired. For the quantitative analysis, the stain was dissolved in 10% cetylpyridinum chloride in 10 mM sodium phosphate (pH 7), and the absorbance was measured at 620 nm.

2.11. Statistical analysis

The data were analyzed using the SPSS 14.0 software (SPSS, USA). A one-way ANOVA test combined with a Student-Newman-Keuls *post hoc* test was used to determine the level of significance. $p < 0.05$ was considered to be significant and $p < 0.01$ was considered to be highly significant.

3. Results

3.1. Surface characterization of QANWAs

Fig. 1A depicts the SEM image of representative TiC/C QANWAs revealing uniform nanowires on the Ti alloy substrate. The density of the nanowires estimated from the SEM image is about 1.0×10^8 cm^{-2}. The TEM image (inset in Fig. 1A) illustrates that the nanowires have a core–shell structure. The core has a uniform diameter of about 40–50 nm and the shell is about 15–20 nm thick. The nanowires have a smooth surface with diameters of 70–90 nm and lengths up to several micrometers. The corresponding XRD pattern of the TiC/C QANWAs is displayed in Fig. 1C (curve 1). The main diffraction peaks can be indexed to cubic TiC (JCPDS card: No 32-1383) except the peaks from the substrate. The TiC/C QANWAs show the characteristics Raman signals of TiC and C as shown in Fig. 1D. The three Raman peaks at approximately 258, 421, and 606 cm^{-1} can be attributed to the vibration signals of TiC [18,19]. The two strong peaks at 1345 cm^{-1} and 1588 cm^{-1} correspond to the D and G bands of carbon, respectively [20]. After annealing in air at 650 °C for 60 min, the samples turn white. The XRD pattern (curve 2 in Fig. 1C) suggests that TiC has been converted into single-crystalline TiO_2. The SEM image in Fig. 1B discloses that the nanowires retain the quasi-aligned array configuration after the C shell has been removed and the core has been converted from TiC to TiO_2.

The water surface contact angles are shown in Fig. 2. The flat Ti6Al4V surface (control) has a water contact angle of 49.25°. The TiC/C QANWAs show superhydrophobicity with a water contact angle of 137.5°, whereas the TiO_2 QANWAs display enhanced hydrophility relative to Ti6Al4V with a water contact angle of 17.2°. The changes in the water contact angles stem from the surface chemistry.

3.2. Protein adsorption

The protein adsorbed from 10% bovine calf serum after 4 h of incubation is assayed and the results are shown in Fig. 3. Although

more protein appears to adsorb onto the QANWAs than Ti6Al4V control, the difference is not statistical significant. There is no appreciable difference in the amount of protein adsorbed on the TiC/C and TiO_2 QANWAs.

3.3. Cytotoxicity assay

The cytotoxicity indicated by the LDH activity in the culture media after 24 h of incubation is assayed and the results are displayed in Fig. 4. The QANWAs show no obvious cytotoxicity compared to the Ti6Al4V control.

3.4. Cell morphology

The SEM pictures in Fig. 5 show the cell morphology on the QANWAs after 3 days of incubation. The cells attach and spread well on the flat surface and after 3 days of culturing, the cells almost completely cover the Ti6Al4V surface. There are many dense lamellipodia and filopodia stretching out to anchor to the surface forming good intercellular connection. In contrast, on the two surfaces with QANWAs, there are only a few cells after 3 days and so the cells cannot grow well on the nanowire surfaces. Compared to the flat control surface, the cells on the QANWA are also much smaller. Some cells on the TiC/C QANWAs are thin and long and they cannot spread well and form solid adhesion. Poorly spreading round cells can also be seen and some cells seem to have an apoptosis appearance of division into small pieces. On the TiO_2 QANWAs, more cells exhibit the apoptosis shape and the rest also exhibit the poorly spring round shape.

3.5. Cell proliferation

The cell proliferation during 4 days of incubation is shown in Fig. 5D. It is obvious that the QANWAs induce a dramatically smaller cell number at days 1 and 4. While the cells proliferate well on the Ti6Al4V surface, the cell number on the QANWAs does not increase with incubation time suggesting impaired proliferation. In fact, after 4 days of incubation, the cell number on the TiC/C or TiO_2 QANWAs is only about 30% of that on the Ti6Al4V control.

3.6. Intracellular total protein synthesis and alkaline phosphatase activity

The intracellular total protein synthesis and alkaline phosphatase activity are signs of cell synthesis ability and early differentiation, respectively and so these two parameters are evaluated with the results shown in Fig. 6. These two parameters are down-regulated on the QANWAs. The intracellular total protein synthesis is severely inhibited to 20% and 35% on the TiC/C and the TiO_2 QANWAs, respectively relative to the flat Ti6Al4V control. The intracellular alkaline phosphatase activity is also depressed dramatically, with a more obvious depression effect on the TiC/C QANWAs to about 45% of that on the flat surface.

3.7. Collagen secretion

Collagen secretion quantified based on Sirius Red staining is shown in Fig. 7. The optical pictures show that collagen secretion by the osteoblasts is drastically reduced on the TiC/C and TiO_2 QANWAs. The collagen secretion on the two QANWAs is about 35–40% of that on the flat Ti6Al4V surface.

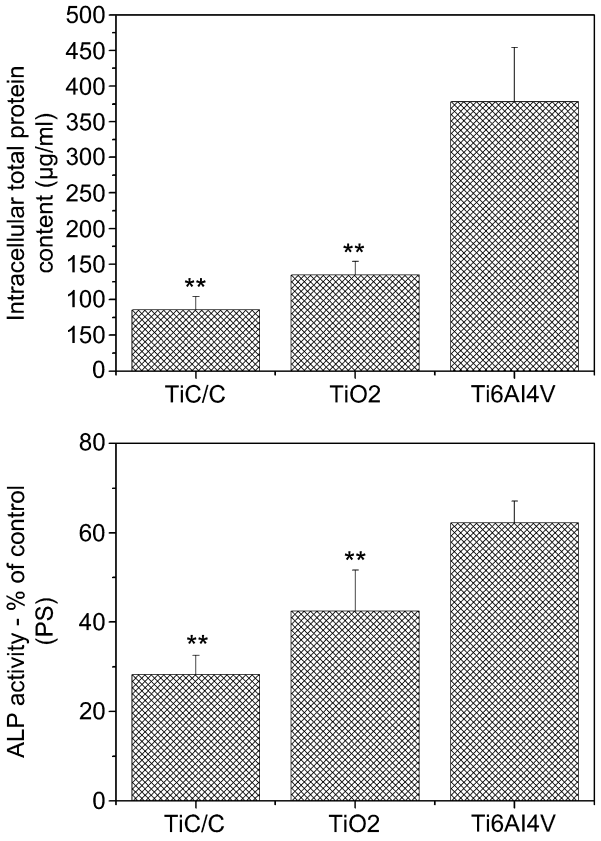

Fig. 6. Intracellular total protein synthesis (top panel) and ALP activity (lower panel) of osteoblasts on the samples after 7 days of incubation. $^{**}p < 0.01$ compared to the flat Ti6Al4V control.

3.8. Extracellular matrix mineralization

The extracellular matrix mineralization measured by Alizarin Red staining is shown in Fig. 8. After 7 days of incubation, there are already many mineralized nodules on the Ti6Al4V control. In contrary, nearly no mineralized nodule can be observed on the two types of QANWAs. The extracellular matrix mineralization on the TiC/C and TiO_2 QANWAs is about 30% of that on the flat surface.

4. Discussion

The experimental results suggest that the QANWAs dramatically reduce cell adhesion, spreading, survival as well as late cell functions such as matrix secretion and mineralization. These effects stem from the QANWAs structure and do not appear to depend on the surface chemistry and surface wettability. Besides, the cell-repelling ability does not stem from reduced protein adsorption as expected. Instead, a little more protein is found to adsorb onto the QANWAs and this phenomenon also does not appear to depend on the difference in surface chemistry. Our data indicate that these QANWAs not only can be used in biosensors or drug releasing systems due to their good biocompatibility, stability, and cell-repelling property, but also provide a good platform to study the effects of nanotopography, surface chemistry, and surface wettability on the biological performance. The latter can provide deeper insight into the mechanisms of cell-repelling and lead to design of better topography to systematically alter cell behaviors.

Anchorage-dependent cells such as osteoblasts need to attach to the extracellular matrix for normal functions or else apoptosis will occur [21,22]. The QANWAs hinder the adhesion of cells as shown

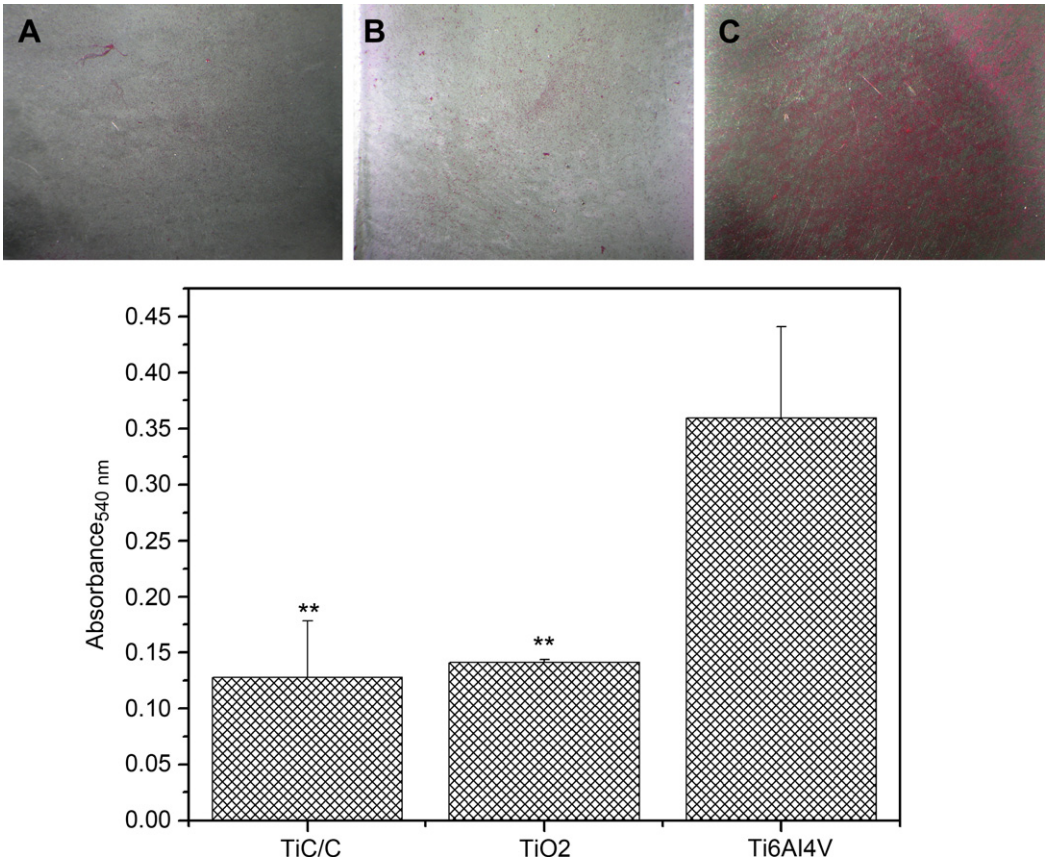

Fig. 7. Collagen secretion by osteoblasts after 7 days of incubation. The top panel displays the optical images: (A) TiC/C QANWAs; (B) TiO_2 QANWAs; (C) flat Ti6Al4V. The lower panel shows the colorimetrically quantitative analysis. $^{**}p < 0.01$ compared to the flat Ti6Al4V control.

by the SEM pictures that cells cannot attach to the nanowire surfaces in a stable fashion and consequently spread poorly on them. Actually, the SEM micrographs indicate many cells appear to undergo apoptosis. Stable cell adhesion to an extracellular matrix provides the signals needed for cell proliferation and differentiation, and good cell proliferation ensures enough differentiated cells in the following stage and good cell-to-cell interactions. All these factors impact the quality and quantity of matrix deposition and biomineralization. The poor cell adhesion and ensuing cell apoptosis explain the small cell number, total intracellular protein synthesis, extracellular matrix secretion, and mineralization. The impeded cell adhesion and low cell survival and matrix deposition finally give rise to a long-lasting anti-biofouling surface in a physiological environment.

In order to rule out the possibility that the smaller cell numbers on the two types of QANWAs may result from the potential toxicity of the QANWAs, we evaluate the cytotoxicity of the QANWAs. The LDH assay in the culture medium after 24 h of incubation shows that the TiC/C and TiO_2 QANWAs are non-cytotoxic as the Ti6Al4V control, suggesting that the dramatically reduced cell numbers is certainly due to the impeded cell functions rather than cytotoxicity. Actually, C and TiO_2 are generally considered to be non-cytotoxic and stable and have in fact been adopted clinically [4,23–25]. Our data suggest that the cell-repelling property of the QANWAs is not due to cytotoxicity and these QANWAs are safe *in vivo*.

The cell attachment and spreading on biomaterials are mediated by a highly complex structure called focal adhesion which is a multi-protein, microscale assembly involving clustering of ligated transmembrane receptor integrins on the nanoscale [26–29]. It has been shown that the spacing between the integrin ligands is important to integrin clustering and focal adhesion [30,31]. There is more evidence that clustering of integrins to assembly requires that the spacing between ligated integrins be less than 50–70 nm [8,9,30–33]. Nanotopographies with spacings larger than 100 nm inhibit cell adhesion [32–34]. In this present study, the nanowires have a diameter of about 70–100 nm, while the distances between nanowires vary from 200 nm to several microns. Hence, although integrin clustering may occur on a single nanowire, the microscale focal adhesion assembly is impaired because of the long distances between nanowires. This mechanism has been adopted by many researchers to explain cell repellence on different nanotopographies [8,9,32,33,35]. The signals from the extracellular matrix transduced via focal adhesion into the cell are very important to cell functions and the shortage leads to eventual cell apoptosis [22,29,36,37].

The cell behavior on biomaterials is strongly related to the surface characteristics of which surface chemistry plays an important role [1]. Here, we evaluate two types of QANWAs with the same topography but different surface chemistry in order to elucidate the mechanism of cell repellence. It is observed that both types of QANWAs effectively prevent cell adhesion and growth in spite of the difference in the surface wettability. Our results are consistent with previous reports. For instance, nanowires [10], nanorods [8,9], and nanoposts [12] which show similar structures as our QANWAs but with different surface chemistry (SiO_2 [8,10,12] and ZnO [9]) have been observed to repel cell adhesion and survival. It has also been reported that polymer rods with diameters of several to hundreds of nanometers [38] and titania pillars with diameters of tens of nanometers [39] inhibit cell functions as their lengths increase. These results indicate the surface structure, not surface chemistry, is the primary factor affecting cell repellence. Hence, other types of QANWAs with similar structures as those

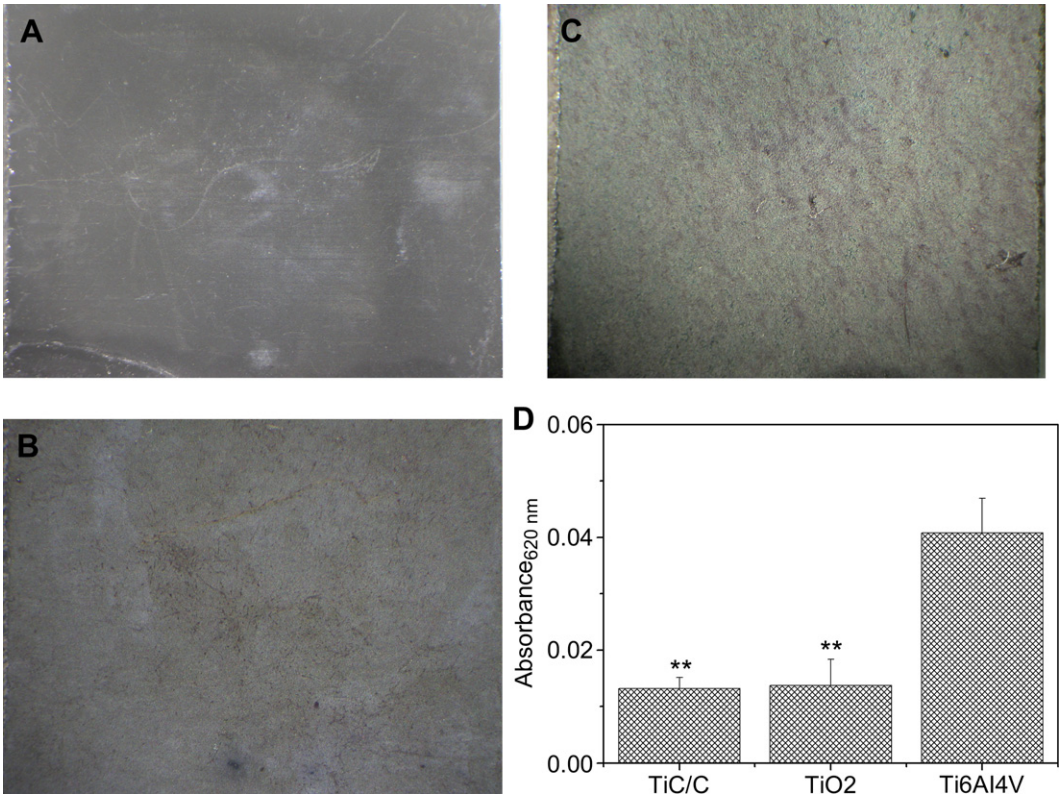

Fig. 8. Extracellular matrix mineralization assayed by staining with Alizarin Red after 7 days of incubation. The optical pictures show the shape of mineralized nodules: (A) TiC/C QANWAs; (B) TiO_2 QANWAs; (C) flat Ti6Al4V. The widely distributed but relatively faint staining in (C) represents the mineralized nodules and the small but distinct staining in (B) is not mineralized nodules but rather discoloration of the samples. (D) shows the colorimetrically quantitative analysis. $^{**}p < 0.01$ compared to the flat Ti6Al4V control.

reported here are expected to repel cell anchorage as well and this technique can be extended to many other nanostructure and substrate combinations.

Surface wettability is also believed to be an important factor in cells/biomaterials interactions as it may influence the cell behavior directly or indirectly by affecting protein adsorption. The surface wettability of the QANWAs is related to the surface chemistry. The TiC/C QANWAs have a superhydrophobic surface with a water contact angle of 137.5° whereas the TiO_2 QANWAs are more hydrophilic relative to the flat Ti6Al4V with a water contact angle of 17.2°. The surface wettability of biomaterials is a complex issue and affected by many factors [40,41]. In this study, as they have the same topography, the wettability difference between the TiC/C and TiO_2 QANWAs can be attributed to the hydrophobic nature of amorphous C and superhydrophilic property of anatase TiO_2 after UV irradiation [42]. The SiO_2 nanowires and SiO_2 coated ZnO nanorods have been found to be superhydrophilic [8,10], and it can be inferred that the SiO_2 nanoposts should also be hydrophilic because of the same surface chemistry and similar surface topography [12]. ZnO nanorods can be hydrophilic or hydrophobic depending on exposure to light [43], but we cannot infer the wettability of ZnO nanorods reported in Ref. [9] due to the complicated substrate preparation procedures. Nonetheless, our study is believed to provide the first evidence that the cell-repelling capability of nanowires has no obvious relationship with surface wettability. There have been efforts to obtain a cell-repelling surface by making the materials surface hydrophobic as it is sometimes believed that a hydrophobic surface can reduce protein adsorption. Compared to chemical modification commonly conducted to create surface hydrophobicity which may degrade gradually in a physiological environment, the topographical technique is more stable and long-lasting in achieving long-term antifouling effects.

Protein adsorption on biomaterials is also considered to play an important role in cells/biomaterials interactions. As aforementioned, there is the speculation that cell repellence can be achieved by designing surfaces that reduce protein adsorption. However, as shown in this study, the QANWAs which show good cell-repelling property do not reduce protein adsorption which is even slightly enhanced on account of the larger surface area on the QANWAs. In fact, similar results have been reported [8]. The reason that higher protein adsorption does not compromise cell repellence is because of the special structure of the vertically aligned nanowires. There is enhanced protein adsorption on the side surface of nanowires but the available ligation sites for cells are still limited to the top area of nanowires. We suppose that more protein can be accumulated among the nanowires even filling the space among the nanowires without impairing cell repellence. Our argument stems from that the formation and growth of focal adhesion is driven by cytoskeletal forces [44,45] and protein accumulation among nanowires may be too pliant to support cell adhesion [46,47] as the underlying substrate is too far away. This presumption is verified by the evidence that the increase in the height of the islands correlates positively with the cell-repelling property [38,39]. This is especially meaningful from the perspective of drug delivery as we can accomplish a high loading capacity for protein drugs while simultaneously keeping the good cell-repelling property. It is of special interest to modulate the protein adsorption and delivery kinetics via possible means such as surface chemistry alteration, although protein adsorption is not shown to be influenced by surface chemistry in this study. More protein loading and controlled release may thus be implemented, and at the same time for better performance in drug delivery, protein adsorption which may compromise the performance of biosensors can be prevented.

5. Conclusion

TiC/C and TiO_2 QANWAs are fabricated on Ti6Al4V alloy. The TiC/C QANWAs show superhydrophobicity whereas the TiO_2 QANWAs are more hydrophilic than the Ti6Al4V control. The two types of QANWAs with different surface chemistry provide a platform to study the contributions of surface nanotopography, surface chemistry, and surface wettability to the cell-repelling property. Our results indicate that both QANWAs impair cell adhesion leading to cell apoptosis possibly by impeding the focal adhesion assembly. Other cell functions such as proliferation and differentiation as monitored by extracellular matrix secretion and mineralization are also obviously inhibited. The cell-repelling property is mainly ascribed to the structure of the QANWAs irrespective of the surface chemistry and surface wettability, suggesting that QANWAs are versatile structures that can be applied to different biomaterials to endow the surfaces with cell-repelling properties. The cell-repelling capability does not origin from reduced protein adsorption because our study reveals that protein adsorption is actually slightly enhanced on the QANWAs probably due to the large surface area on the nanowires. These QANWAs are promising in drug delivery applications and also resist protein adsorption to enhance the performance of biosensors.

Acknowledgements

This work was jointly supported by National High Technology Research and Development Program of China No. 2009AA02Z416, National Natural Science Foundation of China (NSFC 50902104), City University of Hong Kong Strategic Research Grant (SRG) No. 7008009, and Hong Kong Research Grants Council (RGC) General Research Funds (GRF) No. CityU 112307.

Appendix

Figures with essential color discrimination. Figs. 7 and 8 in this article are difficult to interpret in black and white. The full color images can be found in the on-line version, at doi:10.1016/j.biomaterials.2010.07.036.

References

[1] Anselme K. Osteoblast adhesion on biomaterials. Biomaterials 2000;21:667–81.
[2] Mendonca G, Mendonca DB, Aragao FJ, Cooper LF. Advancing dental implant surface technology–from micron- to nanotopography. Biomaterials 2008;29:3822–35.
[3] Mendonca G, Mendonca DB, Simoes LG, Araujo AL, Leite ER, Duarte WR, et al. The effects of implant surface nanoscale features on osteoblast-specific gene expression. Biomaterials 2009;30:4053–62.
[4] Zhao L, Mei S, Wang W, Chu PK, Wu Z, Zhang Y. The role of sterilization in the cytocompatibility of titania nanotubes. Biomaterials 2010;31:2055–63.
[5] Zhao L, Mei S, Chu PK, Zhang Y, Wu Z. The influence of hierarchical hybrid micro/nano-textured titanium surface with titania nanotubes on osteoblast functions. Biomaterials 2010;31:5072–82.
[6] Wei G, Jin Q, Giannobile WV, Ma PX. The enhancement of osteogenesis by nano-fibrous scaffolds incorporating rhBMP-7 nanospheres. Biomaterials 2007;28:2087–96.
[7] Liu X, Smith LA, Hu J, Ma PX. Biomimetic nanofibrous gelatin/apatite composite scaffolds for bone tissue engineering. Biomaterials 2009;30:2252–8.
[8] Lee J, Chu BH, Chen KH, Ren F, Lele TP. Randomly oriented, upright SiO_2 coated nanorods for reduced adhesion of mammalian cells. Biomaterials 2009;30:4488–93.
[9] Lee J, Kang BS, Hicks B, Chancellor Jr TF, Chu BH, Wang HT, et al. The control of cell adhesion and viability by zinc oxide nanorods. Biomaterials 2008;29:3743–9.
[10] Brammer KS, Choi C, Oh S, Cobb CJ, Connelly LS, Loya M, et al. Antibiofouling, sustained antibiotic release by Si nanowire templates. Nano Lett 2009;9:3570–4.
[11] Rahmawan Y, Jang K-J, Moon M-W, Lee K-R, Suh K-Y. Anti-biofouling coating by wrinkled, dual-roughness structures of diamond-like carbon (DLC). Biochip J 2009;3:143–50.
[12] Choi CH, Hagvall SH, Wu BM, Dunn JC, Beygui RE, Kim CJ. Cell interaction with three-dimensional sharp-tip nanotopography. Biomaterials 2007;28:1672–9.
[13] Brinkman SF, Johnston WD. Acute toxicity of aqueous copper, cadmium, and zinc to the mayfly *Rhithrogena hageni*. Arch Environ Contam Toxicol 2008;54:466–72.
[14] Lin W, Xu Y, Huang C-C, Ma Y, Shannon KB, Chen D-R, et al. Toxicity of nano- and micro-sized ZnO particles in human lung epithelial cells. J Nanopart Res 2009;11:25–39.
[15] Zaveri TD, Dolgova NV, Chu BH, Lee J, Wong J, Lele TP, et al. Contributions of surface topography and cytotoxicity to the macrophage response to zinc oxide nanorods. Biomaterials 2010;31:2999–3007.
[16] Huo K, Zhang X, Fu J, Qian G, Xin Y, Zhu B, et al. Synthesis and field emission properties of rutile TiO_2 nanowires arrays grown directly on a Ti metal self-source substrate. J Nanosci Nanotechnol 2009;9:3341–6.
[17] Irie H, Watanabe Y, Hashimoto K. Carbon-doped anatase TiO_2 powders as a visible-light sensitive photocatalyst. Chem Lett 2003;32:772–3.
[18] Klein MV, Holy JA, Williams WS. Raman scattering induced by carbon vacancies in TiCx. Phys Rev B 1978;17:1546–56.
[19] Amer M, Barsoum MW, El-Raghy T, Weiss I, Leclair S, Liptak D. The Raman spectrum of Ti_3SiC_2. J App Phy 1998;84:5817–9.
[20] Ferrari AC, Robertson J. Interpretation of Raman spectra of disordered and amorphous carbon. Phys Rev B 2000;61:14095–107.
[21] Re F, Zanetti A, Sironi M, Polentarutti N, Lanfrancone L, Dejana E, et al. Inhibition of anchorage-dependent cell spreading triggers apoptosis in cultured human endothelial cells. J Cell Biol 1994;127:537–46.
[22] Giancotti FG, Ruoslahti E. Integrin signaling. Science 1999;285:1028–32.
[23] Olivares R, Rodil SE, Arzatec H. Osteoinduction properties of graphite-like amorphous carbon films evaluated in-vitro. Diamond Relat Mater 2007;16:1858–67.
[24] Ruyter IE, Ekstrand K, Bjork N. Development of carbon/graphite fiber reinforced poly (methyl methacrylate) suitable for implant-fixed dental bridges. Dent Mater 1986;2:6–9.
[25] Zhao L, Wei Y, Li J, Han Y, Ye R, Zhang Y. Initial osteoblast functions on Ti-5Zr-3Sn-5Mo-15Nb titanium alloy surfaces modified by microarc oxidation. J Biomed Mater Res A 2010;92:432–40.
[26] Bershadsky A, Kozlov M, Geiger B. Adhesion-mediated mechanosensitivity: a time to experiment, and a time to theorize. Curr Opin Cell Biol 2006;18:472–81.
[27] Yamada KM, Geiger B. Molecular interactions in cell adhesion complexes. Curr Opin Cell Biol 1997;9:76–85.
[28] Maheshwari G, Brown G, Lauffenburger DA, Wells A, Griffith LG. Cell adhesion and motility depend on nanoscale RGD clustering. J Cell Sci 2000;113:1677–86.
[29] Geiger B, Bershadsky A, Pankov R, Yamada KM. Transmembrane crosstalk between the extracellular matrix–cytoskeleton crosstalk. Nat Rev Mol Cell Biol 2001;2:793–805.
[30] Cavalcanti-Adam EA, Volberg T, Micoulet A, Kessler H, Geiger B, Spatz JP. Cell spreading and focal adhesion dynamics are regulated by spacing of integrin ligands. Biophys J 2007;92:2964–74.
[31] Cavalcanti-Adam EA, Micoulet A, Blummel J, Auernheimer J, Kessler H, Spatz JP. Lateral spacing of integrin ligands influences cell spreading and focal adhesion assembly. Eur J Cell Biol 2006;85:219–24.
[32] Park J, Bauer S, von der Mark K, Schmuki P. Nanosize and vitality: TiO_2 nanotube diameter directs cell fate. Nano Lett 2007;7:1686–91.
[33] Park J, Bauer S, Schlegel KA, Neukam FW, von der Mark K, Schmuki P. TiO_2 nanotube surfaces: 15 nm–an optimal length scale of surface topography for cell adhesion and differentiation. Small 2009;5:666–71.
[34] Yim EK, Darling EM, Kulangara K, Guilak F, Leong KW. Nanotopography-induced changes in focal adhesions, cytoskeletal organization, and mechanical properties of human mesenchymal stem cells. Biomaterials 2010;31:1299–306.
[35] Park J, Bauer S, Schmuki P, von der Mark K. Narrow window in nanoscale dependent activation of endothelial cell growth and differentiation on TiO_2 nanotube surfaces. Nano Lett 2009;9:3157–64.
[36] Hynes RO. Integrins: bidirectional, allosteric signaling machines. Cell 2002;110:673–87.
[37] Ben-Ze'ev A, Farmer SR, Penman S. Protein synthesis requires cell-surface contact while nuclear events respond to cell shape in anchorage-dependent fibroblasts. Cell 1980;21:365–72.
[38] Lim JY, Hansen JC, Siedlecki CA, Runt J, Donahue HJ. Human foetal osteoblastic cell response to polymer-demixed nanotopographic interfaces. J R Soc Interface 2005;2:97–108.
[39] Sjostrom T, Dalby MJ, Hart A, Tare R, Oreffo RO, Su B. Fabrication of pillar-like titania nanostructures on titanium and their interactions with human skeletal stem cells. Acta Biomater 2009;5:1433–41.
[40] Lundgren M, Allan NL, Cosgrove T. Modeling of wetting: a study of nano-wetting at rough and heterogeneous surfaces. Langmuir 2007;23:1187–94.
[41] Palasantzas G, De Hosson JTM. Wetting on rough surfaces. Acta Mater 2001;49:3533–8.
[42] Wang R, Hashimoto K, Fujishima A, Chikuni M, Kojima E, Kitamura A, et al. Light-induced amphiphilic surfaces. Nature 1997;388:431–2.

[43] Feng X, Feng L, Jin M, Zhai J, Jiang L, Zhu D. Reversible super-hydrophobicity to super-hydrophilicity transition of aligned ZnO nanorod films. J Am Chem Soc 2004;126:62–3.
[44] Riveline D, Zamir E, Balaban NQ, Schwarz US, Ishizaki T, Narumiya S, et al. Focal contacts as mechanosensors: externally applied local mechanical force induces growth of focal contacts by an mDia1-dependent and ROCK-independent mechanism. J Cell Biol 2001;153:1175–86.
[45] Besser A, Safran SA. Force-induced adsorption and anisotropic growth of focal adhesions. Biophys J 2006;90:3469–84.
[46] McDaniel DP, Shaw GA, Elliott JT, Bhadriraju K, Meuse C, Chung KH, et al. The stiffness of collagen fibrils influences vascular smooth muscle cell phenotype. Biophys J 2007;92:1759–69.
[47] Pelham Jr RJ, Wang Y. Cell locomotion and focal adhesions are regulated by substrate flexibility. Proc Natl Acad Sci U S A 1997;94:13661–5.